JOURNAL OF MATERIALS SCIENCE 33 (1998) 199–206

TEM lattice images and their evaluation by image analysis for activated carbons with disordered microtexture

N. YOSHIZAWA, Y. YAMADA, M. SHIRAISHI
National Institute for Resources and Environment, 16-3 Onogawa, Tsukuba, Japan

Microporous carbons prepared by KOH activation at 400 – 800 °C were observed with transmission electron microscope (TEM). Their microtexture was composed of less-oriented aromatic stacking layers. As the specific surface area was raised with increasing heat-treatment temperature, sinuous layers started to appear. Image analysis technique was applied to the TEM lattice images of the samples for their local regularity by stacking layers. The fast Fourier transformations was utilized to extract a clear image of the stacks from the corresponding lattice image. Furthermore, length (*L*) and number (*N*) of fringes in each stack were automatically measured to quantify their distribution. Their histograms showed the sensitive change of distribution of *N* towards an increase in specific surface area, despite *L* staying unaltered. Accordingly, formation of microtexture responsible for its high surface area was expected to be concerned with decrease in *N* rather than *L* throughout the activation process. Reduction of *N* was further associated with a formation of micropores between layers. The origins of such types of pores were also discussed to show other possibilities than the 'slit-shaped' ones.

1. Introduction

Activated carbons have occupied an important position as adsorbent for a long time. Their capabilities are known to be controlled by some synthesis factors such as origin of carbons, activation method, etc. Further, more precise designs and advancement of them have been investigated. One of the most remarkable studies in recent 20 years is a development and commercialization of activated carbons with effective Brunauer–Emmett–Teller (BET) surface areas over $3000\ m^2\ g^{-1}$ [1]. Such an interesting type of carbon shows lots of potential to extend the application field of activated carbons in the future.

Microscopic structure, or microtexture, of activated carbons has also been investigated in relationship with the adsorption properties. The microtexture of activated carbons is comprised of solid parts made of stacks of aromatic layers, and pores. Adsorption properties of a sample are often connected to the pore structure, which is generally studied by measurement of a molecular adsorption isotherm. However, geometrical states (shape, continuity, etc.) of pores in microtexture cannot be satisfactorily described enough only with an adsorption isotherm. In order to characterize pore systems geometrically, structural analysis of solid parts, serving as pore walls in microtexture, is also required at the same time. Furthermore, structure of the solid part in activated carbon has gathered attentions recently from the point of physical properties such as photoconductivity [2] and random magnetism [3]. However, there are no definite methods for evaluating the solid structure so far because of its complexity, mainly caused by disordered aromatic stacks.

Most studies on the structure of solid part in activated carbon are performed by measuring X-ray diffraction [4], Raman spectrum [5], small-angle X-ray scattering [6] and by observing with transmission electron microscope (TEM) [7–10]. Especially, TEM observation is the most powerful technique for structural analysis of the solid part of activated carbons, because it directly brings visual information on the size and orderings of crystallite. In observation of activated carbons, stacking aromatic layers are generally treated as graphitic crystallites, and thus, denotation of 0 0 2 by Miller index is also used for indicating stacking layers. Investigation of lattice images of chemically activated carbons shows the presence of walls of one to three layers separating cage-like voids [7]. In the 0 0 2 dark-field image, bright dots of 1 nm indicate local parallelism between the aromatic sheets or strips to form slit-shaped pores [8].

Further, the dependence of adsorption behaviour upon those structural features of solid parts is often discussed. The crystallite sizes are expected to be useful parameters for characterizing the microtexture in this case. By TEM observation of 0 0 2 lattice images of activated carbon, some authors have shown that the larger the surface area is, the smaller the number of aromatic layer in stacks is found [9, 10]. Statistical information such as size distribution of crystallite

0022–2461

must clarify the tendency, but it is much more difficult to recognize each crystallite in the whole TEM image.

Here, application of image analysis is one of the best approaches to overcome this problem. Evaluations of TEM micrograph with image analysis have been reported for carbon materials with ordered microtexture [11, 12]. Two-dimensional fast Fourier transform (2D-FFT) seems to be commonly used for ordered structure. Although the microtexture of activated carbons is mostly obscure, it does include the small regularity by aromatic stacks. Therefore, the 2D-FFT algorithm is also expected for characterization of disordered microtexture.

In this paper, it is suggested that image analysis is used for the purpose of quantitative characterization of disordered microtexture of activated carbons at first. Data from the image analysis is also discussed combined with other properties of the sample.

2. Experimental procedure

2.1. Samples

Carbonaceous mesocarbon spherules extracted from coal-tar pitch (mesocarbon microbeads: MCMB, Osaka Gas Co. Ltd.) were mixed with KOH at the weight ratio of KOH/MCMB = 4. The mixture was heated at 3 °C min^{-1} up to 400–800 °C and held at the temperature for 1 h in N_2 flow. After cooling the spherules were washed with diluted HCl and distilled water, and dried in vacuum. Heat-treatment of MCMB without KOH was also performed for comparison. Chemical composition and N_2 adsorption isotherm for each sample was also decided.

2.2. TEM observation and image analysis technique

In TEM (Philips CM30) observation, 0 0 2 lattice images were obtained for powdered samples with accelerating voltage of 300 kV. It is necessary to consider the spherical aberration influence on TEM lattice images, especially in case of objects with high disorder or small crystallite sizes [13]. This point has been discussed in terms of linear transfer theory. The transfer function, $\sin(\chi)$, is often used to express the dependence of image contrast upon the spherical aberration coefficient, C_s, and amount of defocus, Δf, (Equation 1) [14]

$$\sin(\chi) = \sin\left(\frac{\pi}{2}\frac{\lambda^3}{d^4}C_s - \frac{\pi\Delta f}{2}\frac{\lambda}{d^2}\right) \qquad (1)$$

Here, λ is a wavelength of electron beam and d is an interval in real space. Fig. 1 shows the calculated $\sin(\chi)$ for the present observation condition, i.e. $\lambda = 0.00197$ nm and $C_S = 2.0$ mm. By setting the defocus position at $\Delta f = -65$ nm, the maximum contrast for graphitic stacking layers (basal spacing of graphite is 0.34 nm) is obtained. In this case, the image of aromatic stacking layers, are clarified as fringes.

We are not dealing with white regions in 0 0 2 lattice images for our purpose. Microtexture of activated carbons often includes stacking layers less-oriented to each other, as indicated before. These layers can be observed as black fringes if the experimental conditions of TEM are correct. The white region, however, is not always determined as a pore only by the lattice image. In principle, the lattice image is observed when the corresponding lattice planes are exactly positioned according to Bragg's law towards the incident electron beam.

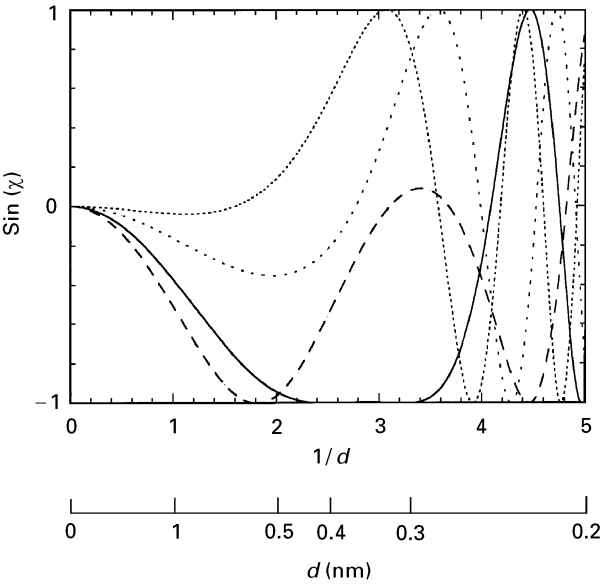

Figure 1 Transfer functions $\sin(\chi)$ at defocus position of -10(· · ·), -30(- - -), -65(——) and -90 nm(– –), respectively, for the experimental parameters described in the text.

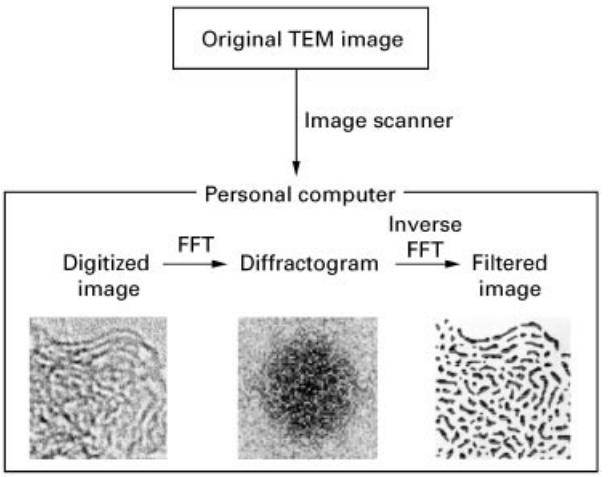

Figure 2 The image analysis process applied to TEM lattice images.

Fig. 2 represents the image analysis procedure used here. The analysing system comprises a personal computer (Apple Macintosh) with an analysis software, an image scanner and output devices.

First, a TEM lattice image is observed with line resolution power of 0.14 nm and at the underfocus position of approximately 65 nm. Then, its positive print is treated with the scanner with the same size as original at 600 d.p.i., to be transformed into a digitized datum. Magnification of the print is a significant factor, which essentially effects the area for an analysis. In order to achieve a good statistical average through the following evaluation of size distribution of stacking

layers, as wide an area as possible must be treated at one procedure. The typical size for a treatment corresponds to 20 × 20 nm in the present work. Each pixel comprising the digitized image indicates its brightness on a scale from 0 to 255.

At the second step in the analysis, 2D-FFT is carried out towards the taken image. The image includes many stacks of aromatic layers as the periodical structure at present; Equation 2 can be used for 2D-FFT calculation

$$F(u, v) = \frac{1}{MN} \sum_{m=0}^{M-1} \sum_{n=0}^{N-1} f(m, n) \times \exp\left[-2i\pi \left(\frac{m}{M} u + \frac{n}{N} v \right) \right] \quad (2)$$

Here $f(m, n)$ represents the information of the real-space image (i.e. the image digitized at the previous step), which is constructed with M and N pixels along the x- and y-axis, respectively. The frequencies, u and v, corresponding to the periodicies along each axis, are used for presenting information of the reciprocal-space diffractogram, $F(u, v)$. A distance between the centre and a point in the diffractogram is proportional to the reciprocal of the period in the real-space image.

Thirdly, the filtering operation is performed on the diffractogram. The operation is effective for sharpening the paralelled fringes by graphitic stacking layers. In detail, the circular regions below 0.3 nm and over 0.5 nm are removed from the diffraction images. The former filtering is for noise reduction, and the latter is to reduce the uneven conditions of contrast in a wide range in the image, respectively.

Finally, the selected region is treated with the inverse 2D-FFT to form a filtered image. The filtered image is constituted only of the fringes caused by the stacking layers with intervals defined above.

3. Results and discussion

3.1. Properties of samples

The origin of 0 0 2 images of the samples is aromatic layers composed of carbon atoms. Elemental analyses show the presence of hydrogen and oxygen especially at samples heat treated below 600 °C, but they are not essentially related to the framework of a layer. For the present purpose of evaluating size distribution of the stacks, a yield of carbon atom for each sample may be referred to. It is determined by chemical composition, and the total yield of each sample, as shown in Fig. 3. Activated samples indicate smaller carbon yield values than non-activated ones at every heat-treatment temperature. Therefore, the presence of KOH surely effects the loss of carbons even at a temperature slightly higher than melting point of KOH (360 °C). It is also shown that the carbon yields are decreased linearly with a rise in temperature for both sample series.

In contrast, the specific surface areas of activated samples characteristically change through heat-treatment. Fig. 4 shows the BET specific surface areas of samples estimated with N_2 adsorption isotherms at − 196 °C. Activation with KOH below 500 °C slightly increases the specific surface areas of samples,

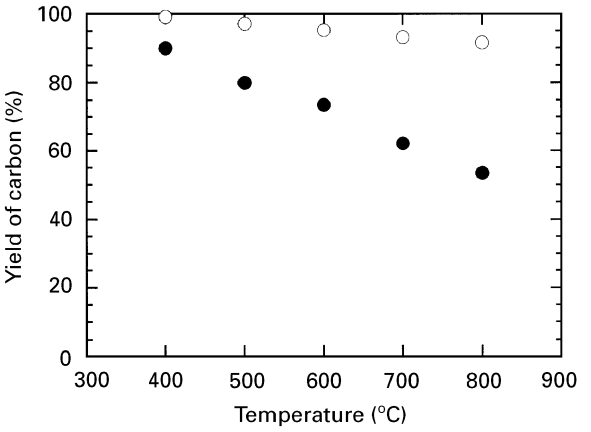

Figure 3 Yields of carbon atom for activated (●) and non-activated (○) samples at each heat-treatment temperature.

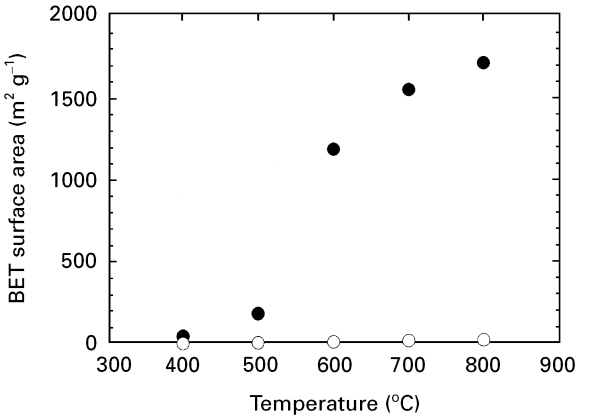

Figure 4 BET specific surface areas of activated (●) and non-activated (○) samples determined by adsorption isotherms of N_2 at −196 °C.

compared to non-activated ones. However, there is a steep rise by sixfold between 500–600 °C, indicating a rapid change of microtextures, which may cause an increase in number of micropores contributing to gas adsorption. Further heat treatment over 600 °C also increases the specific surface areas of the activated samples, but the growth rate does not exceed the one observed between 500–600 °C.

3.2. Lattice image observation with TEM

The 0 0 2 lattice images observed for the non-activated samples (Fig. 5) show the variation of anisotropic microtexture with rising temperature. The sample treated at 800 °C includes column-like structures into which parallel sets of fringes tend to gather with distortion. It is quite a typical aspect of mesophase and has been reported through investigations using X-ray diffraction [15] and TEM observation [16, 17].

On the other hand, microtexture of the activated carbons (Fig. 6) quite differs from one heat-treated at the same temperature without KOH. The preferred orientation found in Fig. 5a is somewhat lost by activation (Fig. 6a) at 400 °C, which may be responsible for the results of the specific surface area. With heat treatment up to 600 °C (Fig. 6b), at which a sharp

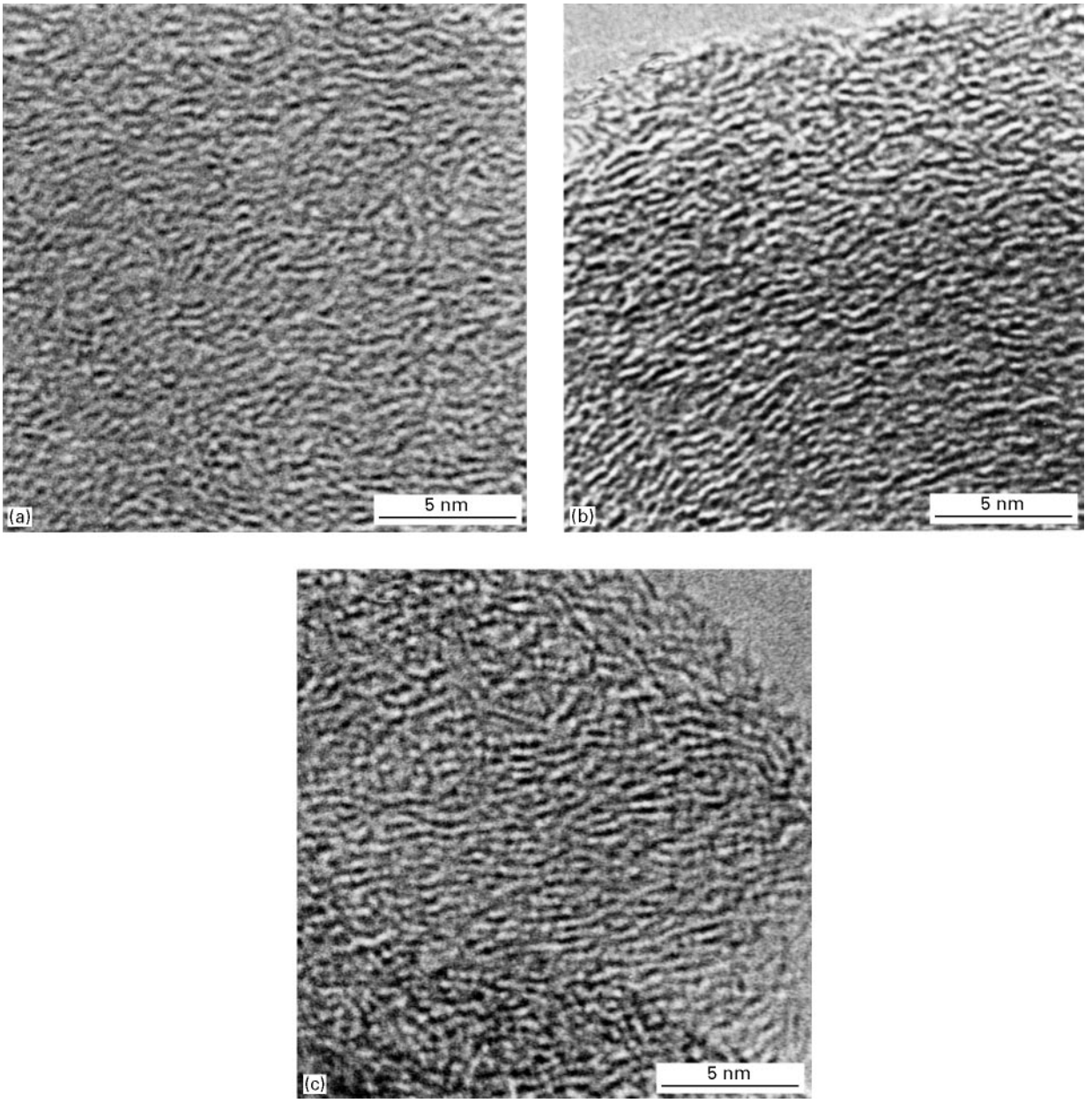

Figure 5 TEM 0 0 2 lattice images of non-activated samples heat-treated at (a) 400 °C, (b) 600 °C and (c) 800 °C.

increase of specific surface area is achieved, some twisted and continuous (~5 nm) fringes start to appear. However, parts of such fringes (~1 nm) are arranged parallel to the adjacent fringe in a strictly local range. These features are emphasized for the activated sample at 800 °C (Fig. 6c). Stacks are arranged along curled lines, so as to surround a domain with 2–3 nm diameter. Also, a couple of parallel layers with fairly large intervals (~0.5 nm) are often found along a long fringe, as shown in Fig. 6d.

3.3. Image analysis of 0 0 2 lattice microphotograph

The image analysis method brings the diffractometry and the filtered image, as already described in Section 2.2. Examples are shown in Fig. 7 for the activated samples. Each diffraction image includes a broad circular pattern in the centre of the diffractogram. If fringes are arranged with orientation in a digitized image, the diffractogram will show an arc-like pattern in the direction of the orientation. However, diffractograms in Fig. 7 are almost isotropic, indicating that fringes in the corresponding digitized image have little orientation of stacks in the analysed region. A diffused pattern like this must be due to small stack sizes in the lattice images. In the filtered images, piled-up fringes are clarified. Intervals of each set of fringes mostly have a range of 0.3–0.5 nm. Through comparison of the filtered image with the original 0 0 2 lattice image at each heat-treatment temperature, appearance of artifacts is not observed. Therefore, it seems reasonable to suppose that our image analysis procedure is valid and effective to extract information from lattice images of disordered carbon microtextures.

In fact, the process used in this paper is theoretically the same as in the case of optical diffractometry and following filtering processing [18]. The optical method is sometimes used for characterizing 0 0 2 lattice fringes of carbon materials. There is an example of

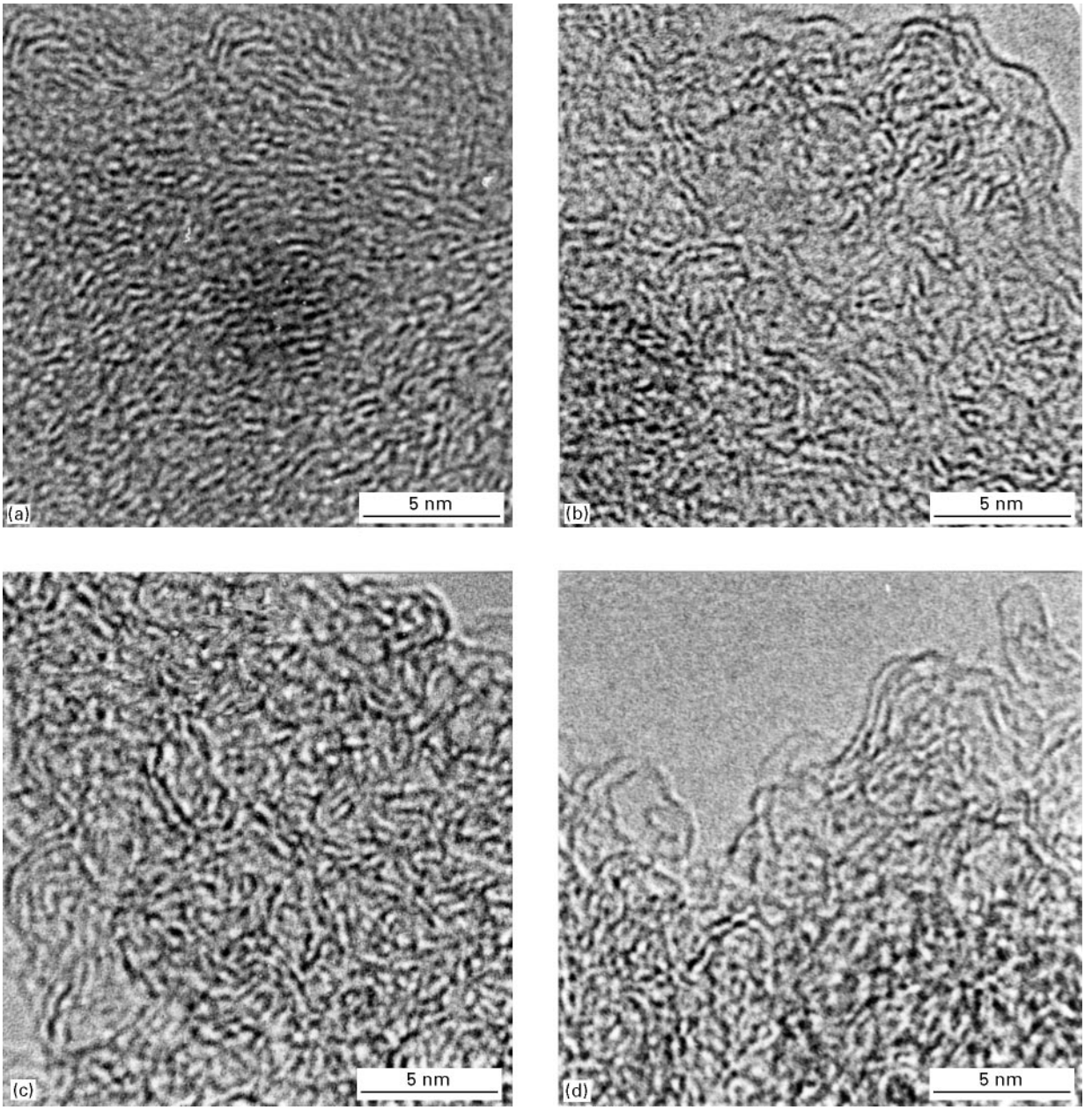

Figure 6 TEM 0 0 2 lattice images of activated samples heat-treated at (a) 400 °C, (b) 600 °C and (c) (d) 800 °C. Parallel layers with basal spacing over 0.5 nm are shown in (d).

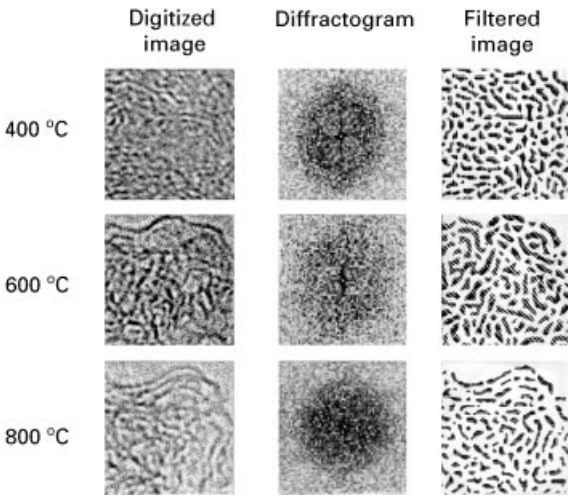

Figure 7 Example of digitized image, diffractogram (diffraction image) and filtered image obtained from 0 0 2 lattice images of activated samples.

the structural study of mesophase spherule with column-like stacking structure by Auguie *et al.* [17]. However, the image analysis seems to have some advantages: for example, simplicity of selection of analytical area, clearness of filtered images and more rapidity for one analysis, when compared with the optical method. It is also worth noting the convenience of following quantitative data acquisition on computer, which is examined in the next paragraph. Of course, both methods including 2D-FFT only treat geometrical information displayed on corresponding images. Thus, the most important factor for correct characterization is the original TEM images taken under an optimal condition.

We further attempt to evaluate the size distribution of the stacks in each filtered image. For the purpose, fringes in the filtered images are classified into apparent stacks (Fig. 8). There are, however, some ambiguities to distinguish exactly which neighbouring unit

a fringe should be assigned to. In this case, a feature of an apparent stack is decided considering the continuity of the interval in both distance and length between adjacent fringes. Next, length of fringe (L) and number of fringes included in them (N) are measured for each stack. The shapes of all apparent stacks have already been digitized as image data at this step, then the parameters like L and N are easily measured on the computer. It is also necessary to say that the data shown below are the average of 10 regions of the same sample, and accordingly, enough to explain the general properties of it.

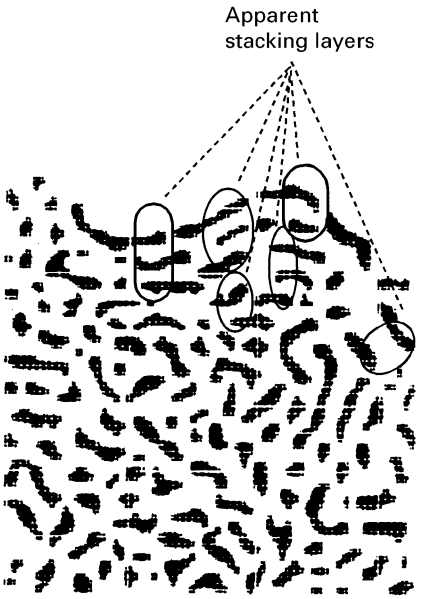

Figure 8 Classification of fringes in filtered image into apparent stacks.

For activated samples, distribution of L is almost similar at 400 and 500 °C, followed by a slight decrease in the ratio of the stacking with $L \geqslant 2.0$ nm. Fig. 9a indicates the histograms of L for the samples activated at 400, 600 and 800 °C, respectively. However, the tendency of the distributions varies little on the whole. Over 50% of the stacking layers ranges of L are between 0.5 and 1.0 nm. Average values of $L(\bar{L})$ in each temperature are also summarized in Table I. The remarkable decrease of $\bar{L}$ from 500–600 °C could be because of the loss of larger fringes stated above. Outside this range, $\bar{L}$ values almost remain unaltered. On the contrary, histograms of the distribution of N obviously depend upon the activation temperature. As shown in Fig. 9b, N distribution keeps its shape below 500 °C, but percentages of stacks with $N \geqslant 4$ fall through heat treatment at 600 °C. Stacks with $N = 2$ rapidly increase their ratio over 50% through heat-treatment from 600 and 800 °C, while stacks with $N > 3$ are entirely reduced. Such a tendency of variation in averaged $N(\bar{N})$ is also expressed in Table I. Especially, the reduction rate of $\bar{N}$ shows its maximum at 500–600 °C. This change of distribution will be discussed in Section 3.4, through comparison with other properties.

Results from the non-activated samples are also summarized in Fig. 10. Histograms of L (Fig. 10a), in each of which the values range wider compared to the

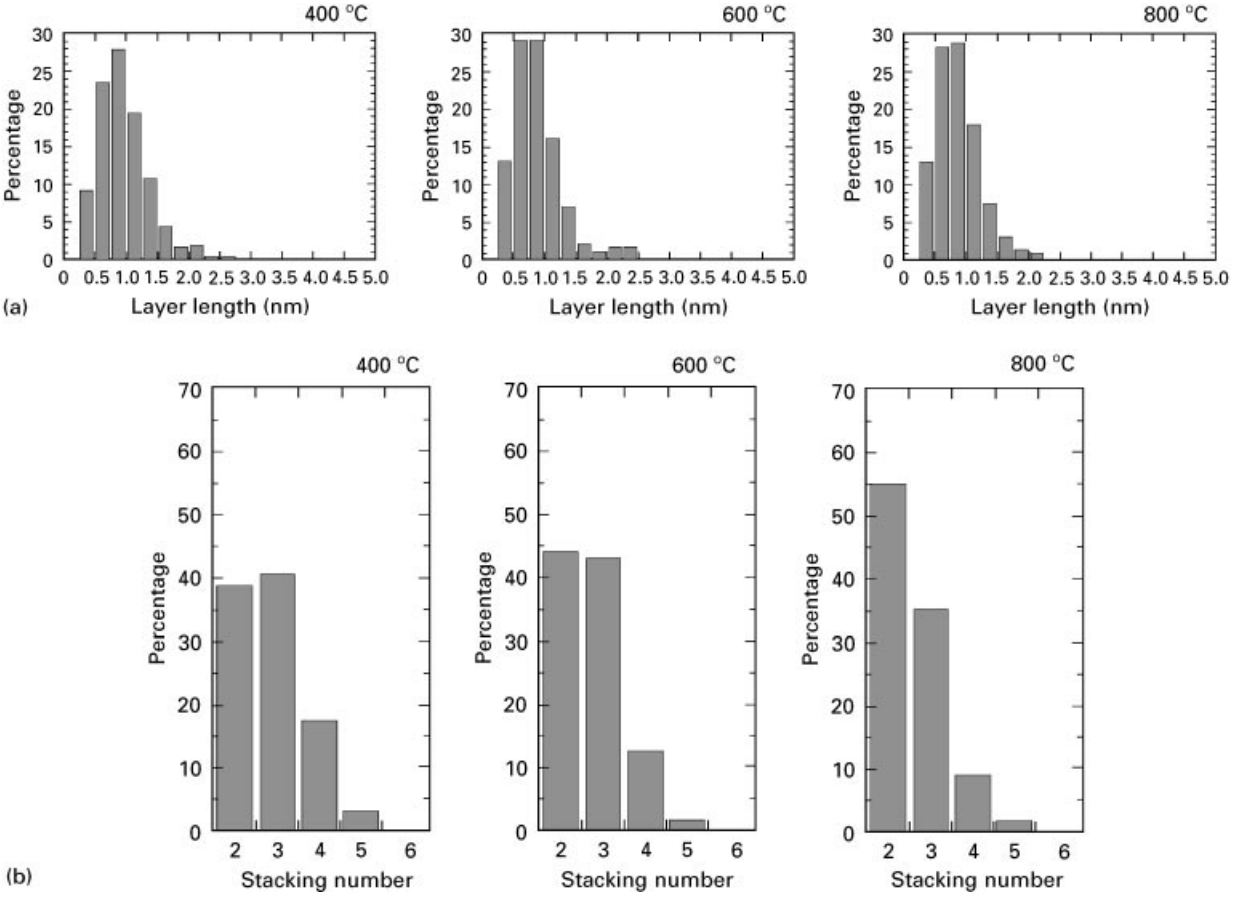

Figure 9 (a) Layer size and (b) number of layer distributions in stacks of activated samples.

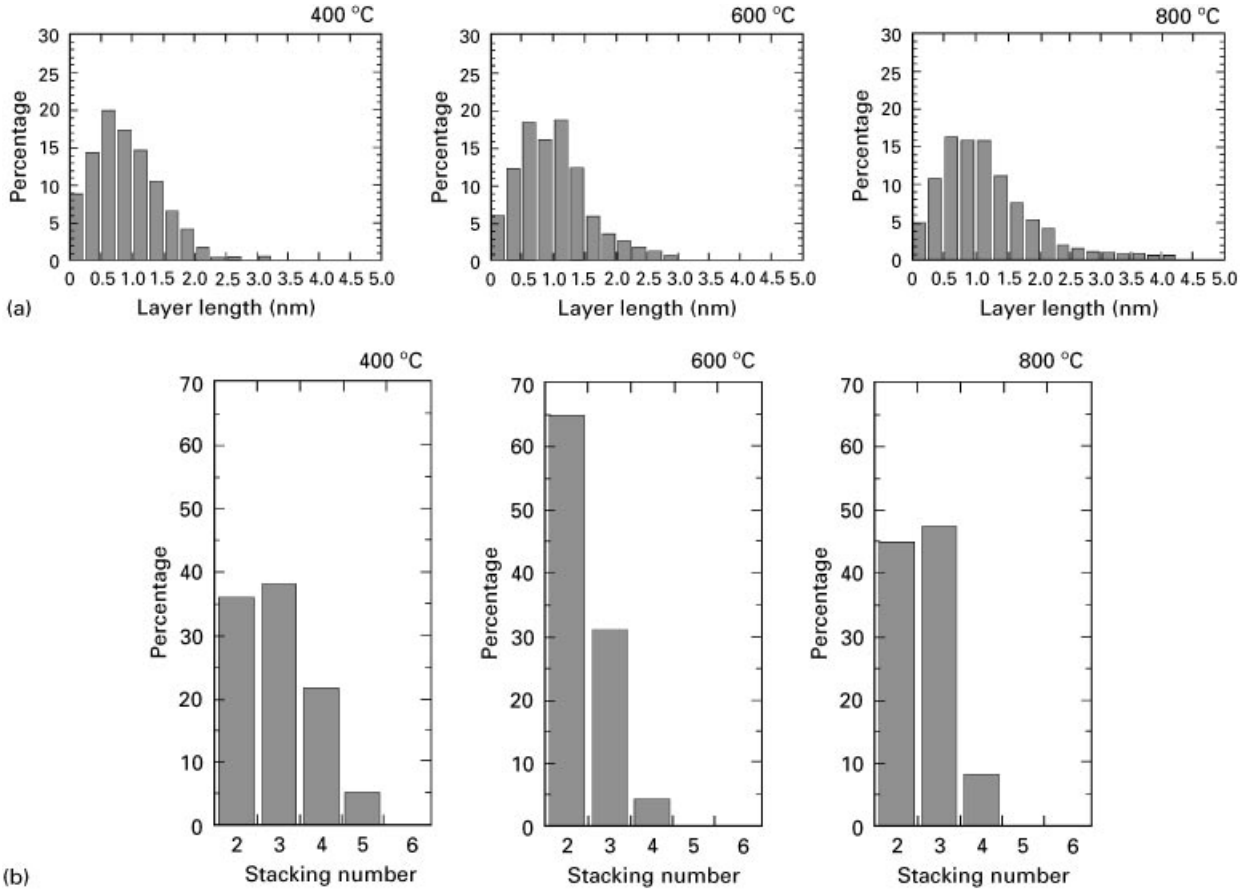

Figure 10 (a) Layer size and (b) number of layer distributions in stacks of non-activated samples.

TABLE I Average width of layers ($\bar{L}$) and number of fringes ($\bar{N}$) included in stacking layers for activated and non-activated samples.

Temperature (°C)	$\bar{L}$ (nm)		$\bar{N}$	
	activated	non-activated	activated	non-activated
400	0.83	079	2.85	2.96
500	0.81	0.83	2.83	2.87
600	0.75	0.89	2.71	2.39
700	0.74	1.17	2.64	2.35
800	0.74	1.25	2.56	2.54

case of the activated samples at the same temperature, shift the distribution maximum to a higher figure with rising temperature. Especially, percentages of $L \geqslant 2.0$ nm are eminently increased through heat treatment. Variation of N seems to be more complicated than that of L, as shown in Fig. 10b. When the temperature is raised up to 600 °C, overall decrease in the ratio of $N \geqslant 3$ and alternative rapid increase of that of $N = 2$ over 60% are clearly illustrated. However, the ratios of $N = 2$ and 3 become closed with heat treatment up to 800 °C.

3.4. Development of high BET surface area and its relationship with crystallite sizes

In this chapter subject is focused on the structure of the activated samples. Details of the activation mechanism with KOH may be found in other studies [19, 20]. For a simple discussion, the activation process performed in our work can be divided into two steps, based on the increase in surface area method shown in Fig. 4. Strictly speaking, surface area is also influenced by a surface condition of a sample. Here, the values of surface area are used simply to show the tendency of structural changes.

In the first step (~ 500 °C) , surface area is slightly raised with increasing temperature. This change attends the decrease in the yield of carbon which is smaller than the non-activated one (Fig. 3). It is obvious to consider the rise of surface area as a result from the loss of carbon by oxidation with KOH. The image analysis indicates that the distributions of L and N are almost similar, regardless of the presence of KOH for each heat-treatment temperature. It suggests that amorphous or disordered carbons not included in stacking layers are the main component of carbon lost in this step.

The second activation step when considered together with a rise of temperature starts between 500 and 600 °C. Here, specific surface area is sharply increased and followed by a continuous rise with elevating temperature. The yield of carbon constantly falls with rising temperature (Fig. 3) and does not correspond to the marked variation of the surface area. Therefore, appearance of microtexture bringing high surface areas should not be characterized only by the lost amount of carbon. According to the image

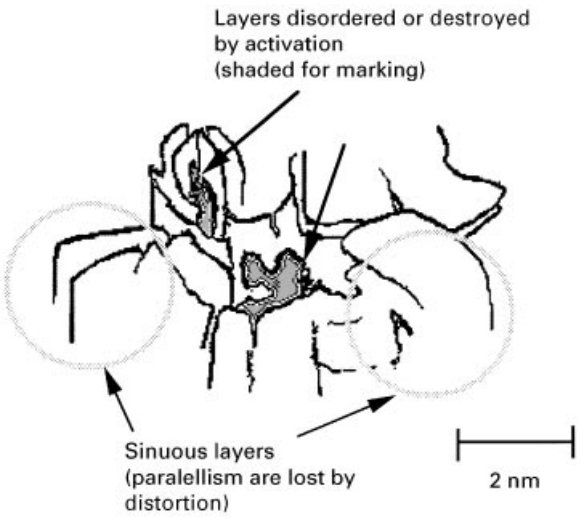

Figure 11 Representative of the microtexture of activated carbon.

analysis of the samples, reduction rate of $\bar{N}$ per 100 °C (Table I) shows its maximum between 500 and 600 °C. It is also found that the $\bar{N}$ value is further decreased up to 800 °C. Such a tendency, indicated by the lost amount of $\bar{N}$, really corresponds to the variation of BET surface area. On the other hand, L is decreased rapidly at 500–600 °C in fact, but not changed in other temperature ranges as mentioned earlier. Therefore, it seems obvious that formation of microtexture responsible for its large surface area is more associated with the decrease in N rather than L throughout the activation process.

A reduction of the number of fringes in the stacks is shown by previous TEM observation of activated carbons [9, 10]. On the other hand, very few reports have been submitted so far with respect to layer sizes.

Decrease in N has been often represented to be the basis of the 'slit-like pore' formed by the complete destruction of aromatic layers in a stack [9]. If this assumption about the shape and formation of micropore is totally true, rise of surface area can be related with the yield of carbon, especially at 500–600 °C. However, our results of carbon yield with a constant decline does not show a good correspondence with characteristic drops of N with increasing surface areas. It means that other explanations should be also offered to describe a porous structure of this type of activated carbon.

Considering that the N reduction is originally found from the result of TEM observation, it is possible that there are some layers which are present in fact, but not observed as fringes because of their distortion or partial destruction, as shown in Fig. 11. Such layers cannot keep their parallelism to adjacent layers, yet they cannot be recognized as lattice fringes. Pores formed like this can be said to be a kind of local defect in stacking structure, rather than slit-shaped ones. The other possibility is concerned with the sinuous layers observed in TEM lattice images; it is also represented in Fig 11. The appearance of such aromatic layers at 600 °C coincides with rise of surface area. Perhaps the piles of layers, especially those with larger size already present at lower temperature, become unable to keep their original shapes through the formation process of the long fringes. Formation of curved layers of the kind can produce strains in stacking structure of piled-up layers, and then cause the reduction of N. Tortions of stacking layers along with such continuous layers play a role of micropore in this case.

4. Conclusions

We have suggested the image analysis technique to evaluate disordered microtexture of activated carbon observed with TEM. This procedure includes the fast Fourier transform algorithm, and utilizes the presence of regularity by small stacks of aromatic layers in the TEM image. It is expected that the technique for characterization of disordered microtexture can be used if an appropriate TEM photograph is taken.

When applied to the lattice image of the samples activated with KOH, the method clarifies the distribution of the layer size (L) and the stacking number of layers (N). In this case the reduction of N rather than L closely corresponds to the generation of high surface area through activation process.

References

1. A. WENNERBERG and T. M. O'GRADY, US Patent (1978) 4, 082, 694.
2. K. KURIYAMA and M. S. DRESSELHAUS, *Phys. Rev.* **B44** (1991) 8256.
3. C. ISHII, Y. MATSUMURA and K. KANEKO, *J. Phys. Chem.* **99** (1995) 5743.
4. J. M. KONNERT and P. D'ANTNIO, *Carbon* **21** (1983) 193.
5. A. M. RAO, A. W. P. FUNG, M. S. DRESSELHAUS and M. ENDO, *J. Mater. Res.* **7** (1992) 1778.
6. N. YOSHIZAWA, Y. YAMADA, M. SHIRAISHI, K. KANEKO and N. SETOYAMA, *J. Chem. Sci. Faraday Trans.* (1996) **92** (1996) 2297.
7. H. MARSH, D. CRAWFORD, T. M. O'GRADY and A. WENNERBERG, *Carbon* **20** (1982) 419.
8. H. F. STOECKLI, *ibid.* **28** (1990) 1.
9. M. HUTTEPAIN and A. OBERLIN, *ibid.* **28** (1990) 103.
10. M. SHIRAISHI, N. YOSHIZAWA, K. OKAWA and T. MAEDA, *Tanso* **155** (1992) 295.
11. K. OSHIDA, M. ENDO, T. NAKAJIMA, S. L. DI VITTORIO, M. S. DRESSELHAUS and G. DRESSELHAUS, *J. Mater. Res.* **8** (1993) 512.
12. M. G. DOBB, H. GUO and D. J. JOHNSON, *Carbon* **33** (1995) 1115.
13. G. R. MILLWARD and D. A. JEFFERSON, in "Chemistry and Physics of Carbon" Vol. 14, edited by P. L. Walker, Jr. and P. A. Thrower (Marcel Dekker Inc., New York, 1978).
14. O. SCHERZER, *J. Appl. Phys.* **20** (1949) 20.
15. A. M. LEVELUT, *J. Phys.* **40** (1979) L81.
16. M. SHIRAISHI, G. TERRIERE and A. OBERLIN, *J. Mater. Sci.* **13** (1978) 702.
17. D. AUGUIE, M. OBERLIN, A. OBERLIN and P. HYVERNAT, *Carbon* **18** (1980) 337.
18. O. KRIVANEK, *Optik* **45** (1976) 97.
19. Y. YAMASHITA and K. OUCHI, *Carbon* **20** (1982) 41.
20. T. OTOWA, R. TANIBATA and M. ITO, *Gas Separation and Purification* **7** (1993) 241.

Received 21 May 1996
and accepted 17 June 1997